

Large-Area Heterostructures from Graphene and Encapsulated Colloidal Quantum Dots via the Langmuir–Blodgett Method

Andrés Black,^{†,‡} Jonathan Roberts,[§] María Acebrón,[†] Ramón Bernardo-Gavito,[§] Ghazi Alsharif,^{§,||} Fernando J. Urbanos,[†] Beatriz H. Juárez,^{†,⊥} Oleg V. Kolosov,[§] Benjamin J. Robinson,[§] Rodolfo Miranda,^{†,‡,‡} Amadeo L. Vázquez de Parga,^{†,‡,‡} Daniel Granados,^{*,†} and Robert J. Young^{*,§}

[†]IMDEA Nanoscience, 28049 Madrid, Spain

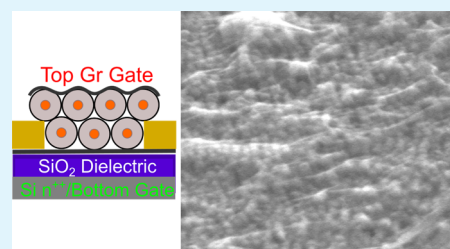
[‡]Departamento de Física de la Materia Condensada, [⊥]Departamento de Química-Física Aplicada, and [#]Condensed Matter Physics Center (IFIMAC), Universidad Autónoma de Madrid, 28049 Madrid, Spain

[§]Physics Department, Lancaster University, Lancaster LA1 4YB, United Kingdom

^{||}Physics Department, Faculty of Science, Taibah University, Tayba, Medina 42353, Saudi Arabia

Supporting Information

ABSTRACT: This work explores the assembly of large-area heterostructures comprised of a film of silica-encapsulated, semiconducting colloidal quantum dots, deposited via the Langmuir–Blodgett method, sandwiched between two graphene sheets. The luminescent, electrically insulating film served as a dielectric, with the top graphene sheet patterned into an electrode and successfully used as a top gate for an underlying graphene field-effect transistor. This heterostructure paves the way for developing novel hybrid optoelectronic devices through the integration of 2D and 0D materials.



KEYWORDS: graphene, colloidal quantum dots, Langmuir–Blodgett, silica encapsulation, surface chemistry

Over the past few decades, low-dimensional materials have garnered scientific attention. In many of them, quantum confinement in one or more directions gives rise to remarkable properties. One such class of materials are 0D semiconducting colloidal quantum dots (CQDs), which have tunable optical and electronic properties that can be tailored by varying the size, shape, and composition of the semiconducting core. The materials surrounding this core can be chosen to mediate the interactions of the CQD with its environment.^{1,2} Graphene (Gr) and other 2D materials, such as transition-metal dichalcogenides, have also been studied extensively and can be combined to form van der Waals heterostructures exhibiting new, unique properties.³ Increased scientific understanding of low-dimensional materials, along with technological advancements in their synthesis and production, has spurred demand for their integration into hybrid quantum systems that combine the remarkable properties of their material components. Heterostructures comprised of CQDs or colloidal nanosheets and graphene are a prime example of such a hybrid quantum system, with numerous studies carried out in the past few years.^{4–9} Energy- and charge-transfer dynamics between these two materials have been explored^{4,5} and exploited to fabricate optoelectronic devices.^{6–9} In all of these studies, the interaction between the graphene and CQDs has been mediated by the organic or inorganic ligands surrounding the CQD semiconducting core. To the best of our knowledge, a hybrid system composed of graphene and silica (SiO₂)-encapsulated semiconducting CQDs has not yet been investigated. These

encapsulated colloidal quantum dots (ECQDs) are attractive because of their increased functionality, solubility in polar solvents, and possible biological applications (because of their decreased toxicity),¹⁰ while maintaining, in some cases, their optical properties.¹¹

This work explores the assembly and characterization of heterostructures comprised of a two-to-three-monolayer ECQD film sandwiched between two graphene sheets, all supported on a SiO₂/silicon (Si) substrate. The bottom graphene sheet can operate as a graphene field-effect transistor (GFET), while the top graphene sheet serves as a top gate, with the two sheets separated by the dielectric ECQD film. Solution-processing methods, used to synthesize the ECQD dielectric film in the heterostructure, are inexpensive, easy to handle, and suited for mass production while allowing for many possible applications.¹² Using transparent graphene as the top electrode allows optical access to the underlying layers. This proof-of-concept hybrid system, or other similar ones assembled using the processes outlined in this paper, could be interesting for several potential scientific investigations or technological applications, such as Stark effect measurements,¹³ resonant tunneling diodes,¹⁴ or photodetectors.¹⁵

Ever mindful of future applications, the techniques used in this work for growing graphene and transferring the ECQD

Received: November 9, 2017

Accepted: February 13, 2018

Published: February 13, 2018

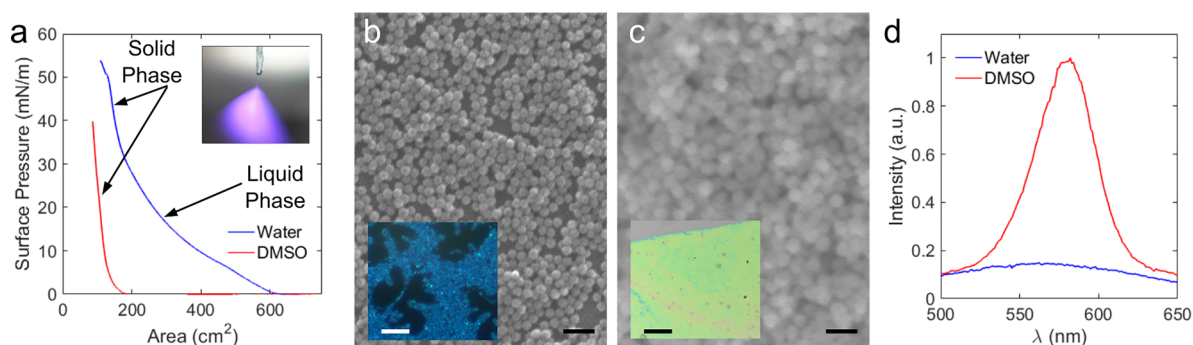


Figure 1. (a) P - A isotherm of ECQD compression on water and DMSO subphases. Inset: Photograph of the ECQD solution electro spray. (b and c) SEM images, with optical images in the inset (dark field in part b and white-light reflection in part c), of ECQD films on a substrate, transferred on (b) water and (c) DMSO subphases. Scale bar = 100 nm. Inset: scale bar = 100 μm . ECQDs in part b have a total diameter of 29 ± 2 nm and those in part c 44 ± 4 nm. (d) PL spectra of ECQD films transferred onto water and DMSO subphases. Excitation wavelength = 300 nm.

films onto the substrate, chemical vapor deposition (CVD) and Langmuir–Blodgett (LB) deposition, are scalable and suitable for producing numerous samples over large areas. The ECQDs used consisted of an alloyed semiconducting core with a CdSe-rich center transitioning to a ZnS-rich outer edge (see Figure S1).¹¹ This alloyed composition gradient eliminates lattice mismatches at abrupt CdSe/ZnS interfaces, which are known to reduce CQD luminescence.^{10,16,17} The semiconducting core is surrounded by organic ligands, critical for the successful growth of an encapsulating amorphous SiO_2 shell via a reverse microemulsion method.¹¹ Unless specifically noted, all experiments were carried out with ECQDs having a total diameter of 44 ± 4 nm. Monolayer graphene, grown on a copper foil in a CVD furnace, was transferred to a SiO_2/Si substrate via a wet etching process, using a poly(methyl methacrylate) (PMMA) stack for mechanical support.¹⁸ Details regarding the ECQD synthesis process, the graphene growth and transfer process, LB deposition, and device fabrication can be found in the Supporting Information.

The LB method is traditionally best suited for depositing amphiphilic molecules in a nonpolar solution using water as a liquid subphase. The solution is normally dispersed onto the subphase as millimeter-sized droplets using a pipet or syringe. Amphiphilic molecules readily spread on the water surface, with the hydrophilic head in contact with the water and the hydrophobic tail pointing away from it.¹⁹ This method is poorly suited for dispersing spherical, nonamphiphilic ECQDs dissolved in relatively high-polarity ethanol onto the subphase, resulting in large losses of material, primarily due to mixing of the polar ethanol and polar subphase. This challenge was overcome by electro spraying the ECQDs (inset Figure 1a) because the resulting micron-sized solution droplets quickly evaporated prior to mixing with the subphase, preventing the ECQDs from sinking.²⁰

The ECQDs floating on the liquid/air interface were physically compressed into films by the LB trough barriers, producing changes in the surface pressure of the subphase liquid as the available surface area was reduced, as shown in the pressure–area (P - A) isotherms in Figure 1a. Initially, water was used as a subphase, and the P - A isotherm showed a gradual increase in the pressure and slope, corresponding to liquid- and solid-like phases in the ECQD film.²¹ Once transferred to a substrate, the resulting films showed a large number of gaps on both the nano- and microscale, as seen in the scanning electron microscopy (SEM) and optical images of Figure 1b. In contrast, by using dimethyl sulfoxide (DMSO) as

the subphase, continuous films were obtained for all length scales (Figure 1c). For electrical applications, a gap-free film is critical for preventing short circuits between the top and bottom graphene sheets of the fabricated heterostructures. The differences in the film morphology for each subphase may have several origins. Apart from the ECQD spheres, a small amount of unencapsulated CQD agglomerates (Figure S1d) and surfactant residues from the synthesis process may be present in the ethanol solution. DMSO's lower polarity and surface tension compared to water may facilitate the elimination of these contaminants.²² DMSO seems to improve the wettability of the SiO_2 spheres, reducing repulsive interactions and allowing for closer packing, as seen in the Brewster angle microscopy images of the ECQD films on a subphase surface (Figure S2a). This reduced interaction would help to explain DMSO's P - A isotherm, with constant zero surface pressure, followed by a sudden jump to the solid phase at the end of the barrier compression.

The photoluminescence (PL) spectra plotted in Figure 1d show that ECQD films deposited on DMSO maintain their luminescent properties (see Figure S1c for spectra in solution), with an emission maximum at 586 nm. In contrast, using water as a subphase completely eliminates the ECQD's luminescence. Similar luminescence quenching, occurring over the course of 2 weeks, has been observed in SiO_2 -coated CdSe nanorods in a water solution upon exposure to ambient oxygen (see also Figure S1c).²³ This is caused by RO^- radicals (e.g., hydroxyls) originating at the water/ SiO_2 interface.^{24–26} The porous nature of SiO_2 shells²⁵ allows the radicals to diffuse toward the ECQD cores, degrading their surface and reducing luminescence. In the LB trough, the ECQDs are located at the air/water interface, where the abundance of oxygen accelerates the radical-forming reaction, leading to very rapid quenching. This result, in addition to the inhomogeneous film coverage, demonstrates that water is not an appropriate subphase for ECQD film deposition.

Having successfully deposited a compact, homogeneous, luminescent film of two-to-three monolayers of ECQDs onto a graphene covered substrate [see atomic force microscopy (AFM) image in Figure S2b], the final step in the heterostructure assembly is transferring a graphene sheet to the top of the ECQD film. DMSO has a strong affinity for graphene and is used as a solvent and exfoliant for graphene sheets in solution.²⁷ Remnants of DMSO on the ECQD film therefore hinder the adhesion of the top graphene sheet. In order to desorb these remnants, samples were heated to 80 $^\circ\text{C}$

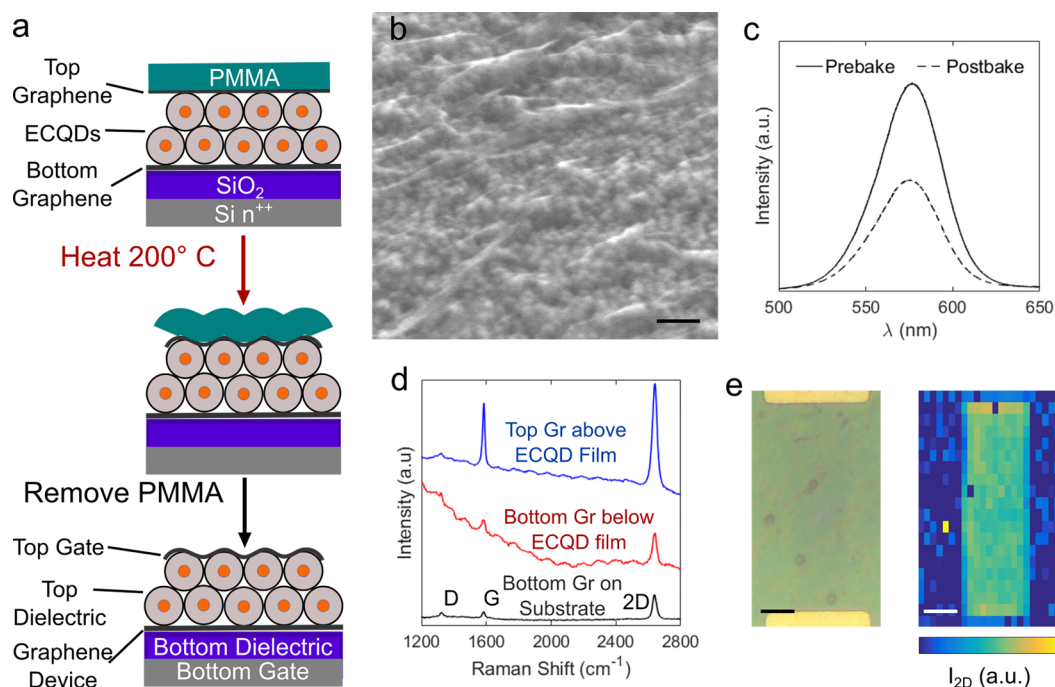


Figure 2. (a) Top graphene-sheet-transfer process, showing material components and the structure of the assembled heterostructure. (b) SEM image of the top graphene on the ECQD film. Scale bar = 100 nm. (c) PL from the ECQD film before and after baking at 200 °C. Excitation wavelength = 488 nm. (d) Raman spectroscopy of graphene on the SiO₂ substrate, below, and above the ECQD film. (e) Optical image of the bottom graphene device below the ECQD film and corresponding Raman spectroscopy map showing a fitted graphene 2D peak intensity. Scale bar = 5 μm. Excitation wavelength in parts d and e = 633 nm.

for 4 h in a 100 mTorr vacuum prior to transferring the top graphene sheet. In addition, after transfer of the graphene sheet but prior to removal of the PMMA supporting film in acetone, the sample was heated to 200 °C for 15 min on a hot plate. This latter step is especially critical, releasing mechanical tensions in PMMA¹⁸ and allowing the graphene to conform and adhere to the underlying ECQD film, as seen in Figure 2a. If this step was not employed, the poorly adhered graphene sheet was largely destroyed upon removal of PMMA. Adhesion was also improved by using small-grain graphene with many grain boundaries (Figure S3). The SEM image in Figure 2b clearly shows the top graphene sheet rippling atop the ECQD film, whose distribution and stacking were practically unaffected by the top graphene-transfer process (Figure S2c). An advantage of using graphene as a top electrode is that it remains suspended over any small imperfections and gaps in the ECQD film, preventing top/bottom electrode short circuits. The PL spectrum from a completed heterostructure in Figure 2c demonstrates that the ECQD film retains its luminescent properties. The loss in the PL intensity is due to ligand degradation exposing surface traps and composition changes in the semiconducting core of the ECQDs,^{1,10} both resulting from high-temperature steps.

Raman spectra and maps of the heterostructure are shown in parts d and e of Figure 2, respectively. The excitation wavelength was set to 633 nm in order to reduce the PL signal from the ECQDs, although the tail end of the PL spectrum is still visible. Even with the ECQDs present, the graphene peaks are still clearly observed, demonstrating that graphene remains unaltered by the heterostructure assembly process. The Raman map depicting the 2D peak intensity of a graphene device demonstrates that the graphene can clearly be detected even when it sits below an ECQD film. The peak

intensity is strongly enhanced for the top graphene sheet, as observed in the blue spectrum in Figure 2e. This is likely the result of small suspended graphene regions, known to result in more intense Raman peaks,²⁸ between the individual ECQD spheres.

AFM and conductive AFM (C-AFM) images, shown in part a and b of Figure 3, respectively, were taken of a heterostructure at the edge of an ECQD film, allowing for comparative measurements in the Gr/ECQD/Gr and Gr/Gr regions. The AFM image reveals the stacking of two 44 nm ECQD layers along the profile line shown in the image, although in some regions three ECQD spheres are stacked. This two-to-three-layer stacking was observed in multiple samples for ECQDs of different sizes and was not altered by transfer of the top graphene sheet (see Figure S2b,c). In C-AFM measurements, a voltage-biased conductive tip comes into contact with the sample while the current is recorded.²⁹ By electrically contacting the bottom graphene sheet and measuring the transmitted current, the vertical resistance in the vicinity of the C-AFM tip is probed. The image in Figure 3b reveals that almost all of the ECQD film is completely electrically insulating, indicating that no current is able to penetrate the insulating SiO₂ shells surrounding the ECQD cores, as expected. The small conducting spot within the Gr/ECQD/Gr region, seen within the blue circle of Figure 3b, is most likely due to a small gap in the ECQD film. These small, isolated spots of conduction, reminiscent of pinholes in dielectric films, were observed very infrequently within the insulating ECQD film.

The electrically insulating nature of the ECQD film allowed for the top graphene sheet to be used as a top-gate electrode for an underlying GFET, as depicted in Figure 2a. The final heterostructure device, after the top graphene sheet was

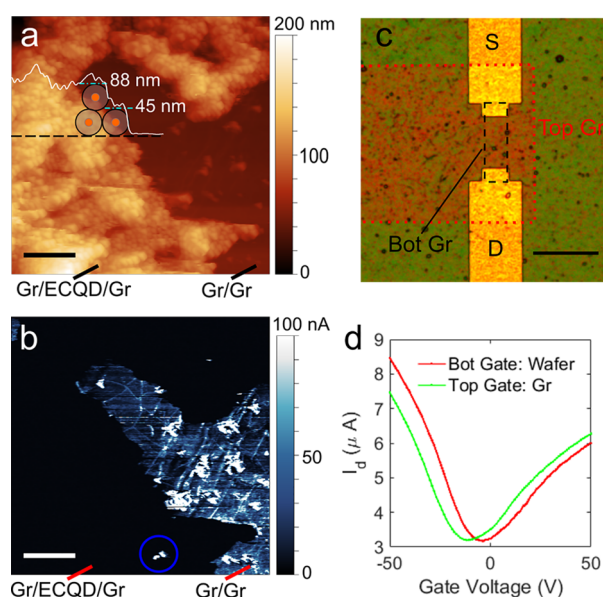


Figure 3. (a and b) Simultaneously acquired AFM and C-AFM images of the heterostructure, showing Gr/Gr and Gr/ECQD/Gr regions. The blue circle in part b shows small conducting spot within the ECQD film region. Scale bar = 500 nm. (c) Optical image of the heterostructure GFET device, with the patterned top graphene sheet acting as a top gate and chromium/gold source and drain (S and D) electrodes. (d) Current modulation with the top and bottom gates.

patterned via photolithography, is shown in Figure 3c. Source–drain current versus gate voltage transfer curves are shown in Figure 3d, modulated by either the bottom gate (the highly doped Si wafer beneath the 285 nm SiO₂ film) or the top graphene electrode gate. Transfer curves measured prior to ECQD film deposition, shown in Figure S4, reveal that the mobility values of the GFET device were reduced (from 350 to 250 V cm² s⁻¹ in the hole branch), likely because of the introduction of defects from the oxygen plasma used to pattern the top graphene sheet. In addition, the doping changed from strongly p type to nearly intrinsic (possibly because of the removal of photoresist contaminants by DMSO), with the Dirac point current minimum occurring at -5 and -12 V for the bottom and top gates, respectively. The transfer curves of four additional devices are shown in Figure S5. The effective relative permittivity of the ECQD film can be calculated using its AFM-measured average thickness and transconductance values obtained from Figure 3d (see the Supporting Information for details), yielding a value of $\epsilon_{\text{ECQD}} = 1.28$. For comparison, the SiO₂ bottom-gate dielectric has a value of $\epsilon_{\text{SiO}_2} = 3.9$. The permittivity of the ECQD films is a volumetric average of the ECQDs and the air between them ($\epsilon_{\text{air}} = 1$); thus, more efficiently packed films will have a larger effective permittivity.³⁰

The large-area heterostructures presented in this work successfully combined for the first time 2D graphene and 0D ECQDs. Using electrospray dispersion and a DMSO subphase to deposit the ECQDs was critical for obtaining homogeneous, gap-free films. After completion of the heterostructure, PL and Raman spectroscopy measurements confirmed that the optical and structural properties of both materials were maintained. The SiO₂ shells of the ECQD films electrically isolated the top and bottom graphene sheets, allowing the top sheet to be used as a gate for a GFET device. The successfully assembled

heterostructures presented in this work pave the way for the development of new optoelectronic devices.

ASSOCIATED CONTENT

Supporting Information

The Supporting Information is available free of charge on the ACS Publications website at DOI: 10.1021/acsami.7b17102.

Details of the experimental methods, supporting figures mentioned in the main text, and details on the calculation of the relative permittivity of the ECQD film (PDF)

AUTHOR INFORMATION

Corresponding Authors

*E-mail: daniel.granados@imdea.org

*E-mail: r.j.young@lancaster.ac.uk

ORCID

Andrés Black: 0000-0002-0726-5357

Oleg V. Kolosov: 0000-0003-3278-9643

Benjamin J. Robinson: 0000-0001-8676-6469

Robert J. Young: 0000-0002-5719-2205

Notes

The authors declare no competing financial interest.

ACKNOWLEDGMENTS

R.J.Y. acknowledges support by the Royal Society through a University Research Fellowship (Grants UF110555 and UF160721). This material is based upon work supported by the Air Force Office of Scientific Research under Award FA9550-16-1-0276. This work was also supported by grants from The Engineering and Physical Sciences Research Council in the U.K. (Grants EP/K50421X/1 and EP/L01548X/1). B.J.R. acknowledges funding from Lancaster University and the Royal Society (Grant RG160834). This work was also partially supported by the Spanish Ministry of Economy, Industry and Competitiveness through Grant FIS2015-67367-C2-1-P, SUPERMAN ESP2015-65597-C4-3-R, and the Comunidad de Madrid through Grants S2013/MIT-3007 MAD2D-CM and S2013/MIT-2740. D.G. acknowledges Grant RYC-2012-09864. A.B. acknowledges Graphene Core Grant H2020-FETFLAG-2014 and a Universidad Autónoma de Madrid FPI scholarship grant. IMDEA Nanociencia acknowledges support from the ‘Severo Ochoa’ Programme for Centres of Excellence in R&D (MINECO, Grant SEV-2016-0686).

REFERENCES

- (1) Kagan, C. R.; Lifshitz, E.; Sargent, E. H.; Talapin, D. V. Building devices from colloidal quantum dots. *Science* **2016**, *353* (6302), aac5523.
- (2) Talapin, D. V.; Lee, J.-S.; Kovalenko, M. V.; Shevchenko, E. V. Prospects of Colloidal Nanocrystals for Electronic and Optoelectronic Applications. *Chem. Rev.* **2010**, *110* (1), 389–458.
- (3) Novoselov, K. S.; Mishchenko, A.; Carvalho, A.; Castro Neto, A. H. 2D materials and van der Waals heterostructures. *Science* **2016**, *353* (6298), aac9439.
- (4) Chen, Z.; Berciaud, S.; Nuckolls, C.; Heinz, T. F.; Brus, L. E. Energy Transfer from Individual Semiconductor Nanocrystals to Graphene. *ACS Nano* **2010**, *4* (5), 2964–2968.
- (5) Ajayi, O. A.; Anderson, N. C.; Cotlet, M.; Petrone, N.; Gu, T.; Wolcott, A.; Gesuele, F.; Hone, J.; Owen, J. S.; Wong, C. W. Time-resolved energy transfer from single chloride-terminated nanocrystals to graphene. *Appl. Phys. Lett.* **2014**, *104* (17), 171101.
- (6) Sun, Z.; Liu, Z.; Li, J.; Tai, G.-a.; Lau, S.-P.; Yan, F. Infrared Photodetectors Based on CVD-Grown Graphene and PbS Quantum

Dots with Ultrahigh Responsivity. *Adv. Mater.* **2012**, *24* (43), 5878–5883.

(7) Konstantatos, G.; Badioli, M.; Gaudreau, L.; Osmond, J.; Bernechea, M.; de Arquer, F. P. G.; Gatti, F.; Koppens, F. H. L. Hybrid graphene-quantum dot phototransistors with ultrahigh gain. *Nat. Nanotechnol.* **2012**, *7* (6), 363–368.

(8) Nikitskiy, I.; Goossens, S.; Kufer, D.; Lasanta, T.; Navickaite, G.; Koppens, F. H. L.; Konstantatos, G. Integrating an electrically active colloidal quantum dot photodiode with a graphene phototransistor. *Nat. Commun.* **2016**, *7*, 11954.

(9) Robin, A.; Lhuillier, E.; Xu, X. Z.; Ithurria, S.; Aubin, H.; Ouerghi, A.; Dubertret, B. Engineering the Charge Transfer in all 2D Graphene-Nanoplatelets Heterostructure Photodetectors. *Sci. Rep.* **2016**, *6*, 24909.

(10) Donega, C. d. M. Synthesis and properties of colloidal heteronanocrystals. *Chem. Soc. Rev.* **2011**, *40* (3), 1512–1546.

(11) Acebrón, M. a.; Galisteo-López, J. F.; Granados, D.; López-Ogalla, J.; Gallego, J. M.; Otero, R.; López, C.; Juárez, B. H. Protective Ligand Shells for Luminescent SiO₂-Coated Alloyed Semiconductor Nanocrystals. *ACS Appl. Mater. Interfaces* **2015**, *7* (12), 6935–6945.

(12) Konstantatos, G.; Sargent, E. H. Nanostructured materials for photon detection. *Nat. Nanotechnol.* **2010**, *5*, 391.

(13) Scott, R.; Achtstein, A. W.; Prudnikau, A. V.; Antanovich, A.; Siebbeles, L. D. A.; Artemyev, M.; Woggon, U. Time-Resolved Stark Spectroscopy in CdSe Nanoplatelets: Exciton Binding Energy, Polarizability, and Field-Dependent Radiative Rates. *Nano Lett.* **2016**, *16* (10), 6576–6583.

(14) Roberts, J.; Bagci, I. E.; Zawawi, M. A. M.; Sexton, J.; Hulbert, N.; Noori, Y. J.; Young, M. P.; Woodhead, C. S.; Missous, M.; Migliorato, M. A.; Roedig, U.; Young, R. J. Using Quantum Confinement to Uniquely Identify Devices. *Sci. Rep.* **2015**, *5*, 16456.

(15) Kim, S.; Shin, D. H.; Kim, J.; Jang, C. W.; Kang, S. S.; Kim, J. M.; Kim, J. H.; Lee, D. H.; Kim, J. H.; Choi, S.-H.; Hwang, S. W. Energy transfer from an individual silica nanoparticle to graphene quantum dots and resulting enhancement of photodetector responsivity. *Sci. Rep.* **2016**, *6*, 27145.

(16) Efros, A. L.; Nesbitt, D. J. Origin and control of blinking in quantum dots. *Nat. Nanotechnol.* **2016**, *11* (8), 661–671.

(17) Bae, W. K.; Padilha, L. A.; Park, Y.-S.; McDaniel, H.; Robel, L.; Pietryga, J. M.; Klimov, V. I. Controlled Alloying of the Core–Shell Interface in CdSe/CdS Quantum Dots for Suppression of Auger Recombination. *ACS Nano* **2013**, *7* (4), 3411–3419.

(18) Suk, J. W.; Kitt, A.; Magnuson, C. W.; Hao, Y.; Ahmed, S.; An, J.; Swan, A. K.; Goldberg, B. B.; Ruoff, R. S. Transfer of CVD-Grown Monolayer Graphene onto Arbitrary Substrates. *ACS Nano* **2011**, *5* (9), 6916–6924.

(19) Ariga, K.; Yamauchi, Y.; Mori, T.; Hill, J. P. 25th Anniversary Article: What Can Be Done with the Langmuir–Blodgett Method? Recent Developments and its Critical Role in Materials Science. *Adv. Mater.* **2013**, *25* (45), 6477–6512.

(20) Nie, H.-L.; Dou, X.; Tang, Z.; Jang, H. D.; Huang, J. High-Yield Spreading of Water-Miscible Solvents on Water for Langmuir–Blodgett Assembly. *J. Am. Chem. Soc.* **2015**, *137* (33), 10683–10688.

(21) Talham, D. R. Conducting and Magnetic Langmuir–Blodgett Films. *Chem. Rev.* **2004**, *104* (11), 5479–5502.

(22) Aleksandrovic, V.; Greshnykh, D.; Randjelovic, I.; Frömsdorf, A.; Kornowski, A.; Roth, S. V.; Klinke, C.; Weller, H. Preparation and Electrical Properties of Cobalt–Platinum Nanoparticle Monolayers Deposited by the Langmuir–Blodgett Technique. *ACS Nano* **2008**, *2* (6), 1123–1130.

(23) Pietra, F.; van Dijk - Moes, R. J. A.; Ke, X.; Bals, S.; Van Tendeloo, G.; de Mello Donega, C.; Vanmaekelbergh, D. Synthesis of Highly Luminescent Silica-Coated CdSe/CdS Nanorods. *Chem. Mater.* **2013**, *25* (17), 3427–3434.

(24) Zhang, H.; Dunphy, D. R.; Jiang, X.; Meng, H.; Sun, B.; Tarn, D.; Xue, M.; Wang, X.; Lin, S.; Ji, Z.; Li, R.; Garcia, F. L.; Yang, J.; Kirk, M. L.; Xia, T.; Zink, J. I.; Nel, A.; Brinker, C. J. Processing Pathway Dependence of Amorphous Silica Nanoparticle Toxicity:

Colloidal vs Pyrolytic. *J. Am. Chem. Soc.* **2012**, *134* (38), 15790–15804.

(25) Darbandi, M.; Urban, G.; Krüger, M. A facile synthesis method to silica coated CdSe/ZnS nanocomposites with tuneable size and optical properties. *J. Colloid Interface Sci.* **2010**, *351* (1), 30–34.

(26) Cavaliere-Jaricot, S.; Darbandi, M.; Nann, T. Au-silica nanoparticles by “reverse” synthesis of cores in hollow silica shells. *Chem. Commun.* **2007**, No. 20, 2031–2033.

(27) Johnson, D. W.; Dobson, B. P.; Coleman, K. S. A manufacturing perspective on graphene dispersions. *Curr. Opin. Colloid Interface Sci.* **2015**, *20* (5), 367–382.

(28) Berciaud, S.; Ryu, S.; Brus, L. E.; Heinz, T. F. Probing the Intrinsic Properties of Exfoliated Graphene: Raman Spectroscopy of Free-Standing Monolayers. *Nano Lett.* **2009**, *9* (1), 346–352.

(29) Mativetsky, J. M.; Loo, Y.-L.; Samori, P. Elucidating the nanoscale origins of organic electronic function by conductive atomic force microscopy. *J. Mater. Chem. C* **2014**, *2* (17), 3118–3128.

(30) Deák, A.; Bancsi, B.; Tóth, A. L.; Kovács, A. L.; Hörvölgyi, Z. Complex Langmuir–Blodgett films from silica nanoparticles: An optical spectroscopy study. *Colloids Surf., A* **2006**, *278* (1), 10–16.